Journal of Ovonic Research Vol. 18, No. 6, November - December 2022, p. 739 - 751

Structural, optical and magnetic properties of dilute magnetic semiconductor of $Zn_{1-x}Ni_xO$ thin films for spintronic devices

M. Ahmed[a,*], A. Bakry[a], H. Dalir[b], E. R. Shaaban
[a]*Department of Physics, Faculty of Science, King Abdulaziz University, 80203 Jeddah21589, Saudi Arabia*
[b]*Department of Electrical and Computer Engineering, George Washington University, 20052, Washington, D.C., USA*
[c]*Physics Department: Faculty of Science, Al-Azhar University, P.O. 71452, Assiut, Egypt*

Co-precipitation method is used to create various compositions of the bulk sample of Zn1-xNixO (x = 0, 0.02, 0.04, 0.06, 0.08, and 0.1). By using an electron beam approach, the required coatings were deposited onto extremely clean glass substrates. The current study examines the structural and optical, characteristics of Ni-doped ZnO thin films. The creation of the hexagonal wurtzite single phase of ZnO was revealed by X-ray diffraction, and it had a strong (002) peak with a peak shift towards a lower angle. It was discovered that the films' crystallite size shrank as the Ni content rose. Investigations were done into how Ni dopant affected the produced thin films' optical and magnetic properties. The optical energy gap decreases from 3.28 to 2.90eV with increasing Ni content. In addition, ferromagnetism increases with increasing Ni concentration at expense of Zn in Zn1-xNixO films . The changes in the optical and magnetic properties of the prepared films were discussed based on the structural modification, which, further, enhances upon Ni-doping.

(Received August 28, 2022; November 8, 2022)

Keywords: $Zn_{1-x}Ni_xO$ thin films, Structure parameters, Optical, Energy gap, Ferromagnetism

1. Introduction

ZnO has interesting properties such as wide band gap (3.37 eV) with large exciton binding energy (60 meV), low dielectric constant, high chemical stability, large electrochemical coupling coefficient, high thermal conductivity and UV protection [1-3]. ZnO films possess high transmittance in the visible and infrared spectral regions and high refractive index, which extend their application range. Recently, diluted magnetic semiconductor (DMS) attracted the attention because of their unique properties such as electronic, magnetic and magneto-optical properties [4, 5]. Their structural, electrical and optical properties can be varied by tunability of lattice parameters, microstructural parameters and energy gaps with respect to the concentration of transition metal (TM) [6, 7]. But, generating reproducible long-range ferromagnetism (FM) in wide bandgap-DMS materials still a major obstacle to the fabrication of spintronic devices operating above room temperature [7, 8]. ZnO is well-known as n-type semiconductor where its electrical conductivity is due to the excess of zinc interstitial position [9]. Also, ZnO doped with Cr, Mn, Fe and Ni has showed novel attention due to the strong correlation between the structural, optical, and magnetic properties [10, 11]. Doping with various amount of Ni not only enhances electron-hole pair separation by decrease the band gap to make advantages of shifting the absorption to the visible light spectrum, but also decrease the average grain size [12,13]. In addition, a unique feature of nanostructures is the large surface to volume ratio available in these systems. They consist of grains, grain boundaries and grain interfaces w ich play important role in the determination of the electrical properties [14–17]. It is also well-known that the interior defects such as A-site vacancies, space charge electrons or oxygen vacancies have great influence on electrics, dielectrics and optical properties, and they are

---

[*] Corresponding author: mhafidh@kau.edu.sa

https://doi.org/10.15251/JOR.2022.186.739

very important to gain a fundamental understanding of these properties. In this study, we have used Ni doping to improve the optical and electrical properties of ZnO material. The aim of the present work is to study the role of Ni-doping and defects on the structural, optical and magnetic properties of Ni:ZnO thin films for spintronics applications.

2. Experimental

Different compositions of the bulk samples of $Zn_{1-x}Ni_xO$ (x = 0, 0.02, 0.04, 0.06, 0.08, and 0.1) were fabricated using co-precipitation technique of $Zn(NO_3)_2.6H_2O$ with the appropriate amount of $Ni(NO_3)_3.6H_2O$ to make the required doping percentage dissolved in 50 ml of distilled water. Zinc and Gadolinium nitrates are dissolved in deionized water and then kept stirring for 1 hour. NH_4OH solution was added dropwise till the pH of the solution has reached 9. This mixture was stirred for 2 hours at room temperature and, consequently, filtered. The precipitate was dried at 80 ^oC for 4 hours.

The thermogravimetric analysis (TGA) (Shimadzu 50) of the precursor was performed. According to TGA analysis, the calcination temperature was chosen to be 564 ^oC for 2 hours in order to get a polycrystalline powder. Different $Zn_{1-x}Ni_xO$ thin films with the same thickness were evaporated in terms of electron beam gun technique with a vacuum of about 10^{-6} Pa. The evaporation rate, as well as film thickness, was controlled using a quartz crystal FTM6 monitor. The deposition rate was maintained constant at about 2 nm/s during the sample preparation. Such a low deposition rate can produce a film with a composition very close to that of the bulk starting material.

The structure of the powder and thin films of $Zn_{1-x}Ni_xO$ were measured using X-ray diffraction (XRD, Shimadzu X-ray diffractometry 6000, Japan) with Cu-K_α radiation having λ = 0.15418 nm. The intensity data was collected by step scan modes of a 2θ range between 5^o and 70^o with a step size of 0.02^o and step time of 0.6 s. The pure silicon (≈ Si 99.9999 %) is used as an internal standard. The composition of the synthesized polycrystalline particles is quantified by energy-dispersive analysis of X-ray (EDAX) using energy-dispersive X-ray (EDX) spectrometer. The optical transmittance of the deposited films is measured using a UV-VIS-NIR JASCO V-670 double-beam spectrophotometer. The transmittance spectra in the wavelength range of 300-2500 nm were collected at normal incidence without a substrate in the reference beam. The magnetic properties of the prepared films were studied using the vibrating sample magnetometer model (VSM-9600M-1, USA). The measurements were conducted at room temperature in a maximum applied field of 15 kOe.

3. Results and discussion

3.1. Structural properties

To research the thermal behaviour of precursor materials, one of the most important thermal analysis techniques is TGA. As depicted in Fig. 1, TGA was performed at temperatures ranging from ambient temperature to 700 °C. According to this data, the subsequent phases resulted in a weight loss of 15%, with the first phase's weight loss of 1.5% being attributable to the removal of water that had been adsorbed on the material's surface. The second happened between 98 and 360 degrees Celsius, where there was a weight loss of around 5.5% that was caused by the evaporation of organic contaminants. The final weight loss, which was roughly 6% and happened between 360 and 564 °C, may be attributed to zinc oxide's full crystallisation from its amorphous state. The remaining fourth weight loss about 1% is due to the oxidation of residue compounds.

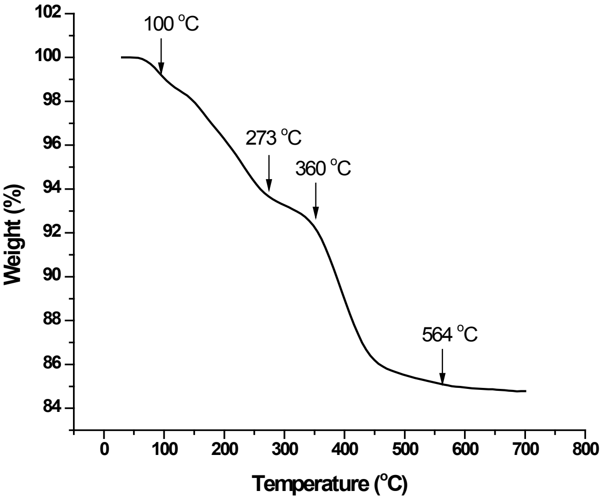

Fig. 1. Thermogravimetric analysis of the precursor.

The EDAX spectra of the thin films Zn0.98Ni0.02O and Zn0.90Ni0.10O, respectively, are depicted in Fig 2. The appearing peaks show the stoichiometry of the Zn, O, and Ni content. The Ni2+ ions' successful acceptor assimilation into the Zn lattice is shown by an increase in Ni concentrations in Zn1-xNixO films. These findings are fairly consistent with the experimental setup being used in the system at hand. The purity of the film sample is confirmed by the lack of additional components in the spectra.

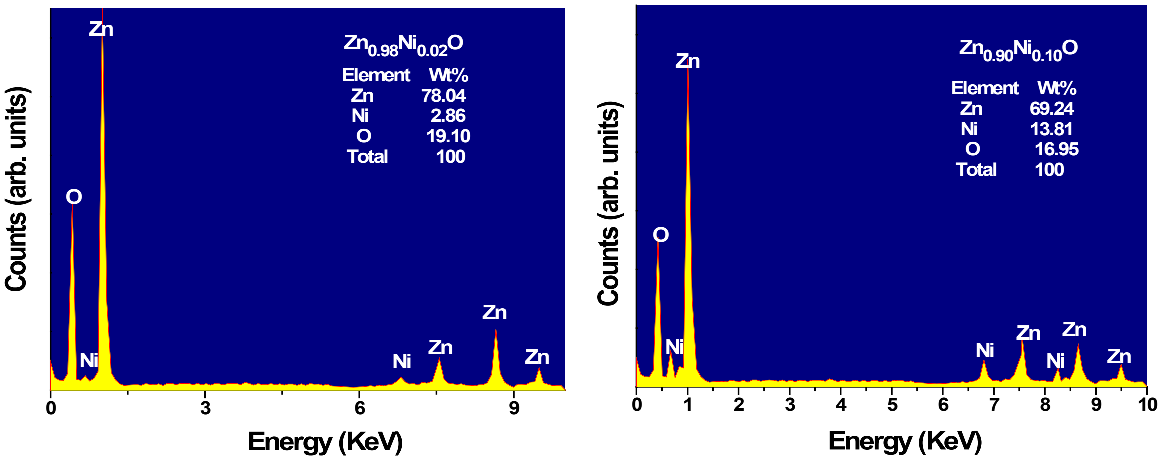

Fig. 1. EDAX spectra of ZnO doped with Cu thin film (a) $Zn_{0.98}Ni_{0.02}O$ *(b)* $Zn_{0.90}Ni_{0.10}O$*.*

Zn1-xNixO thin film XRD patterns and typical JCPDS data were compared. The hexagonal wurtzite ZnO structure (JCPDS 01-1136) is properly indexed to all of the diffraction peaks, demonstrating that Ni doping has no effect on the crystal structure of ZnO. The production of the Zn1-xNixO solid is confirmed by the XRD pattern's lack of any Ni traces or other impurity phase diffraction peaks. Additionally, Figure 3 demonstrates that when Ni concentration rises, the intensity of the favoured orientation (002) plane peaks weakens and shifts toward lower values of the diffraction angle (see Fig. 4). Because Ni2+ ions have shorter ionic radii (r = 0.070 nm) than Zn2+ ions (r = 0.074 nm), the peak position has been shifted.

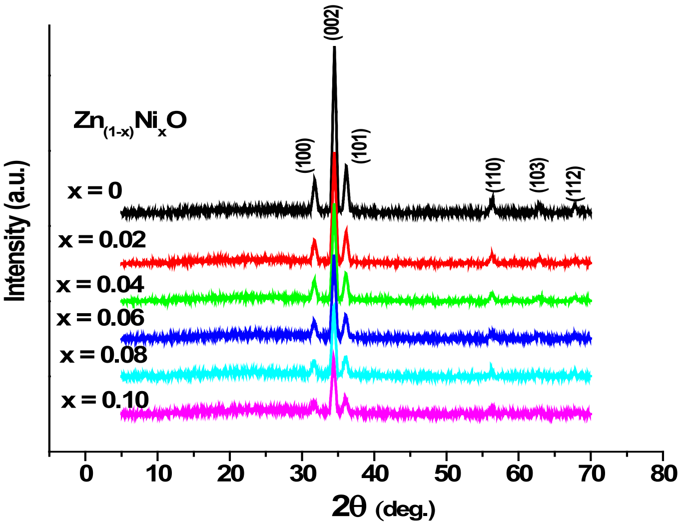

Fig. 3. X-ray diffraction patterns of polycrystalline $Zn_{1-x}Ni_xO$ thin films.

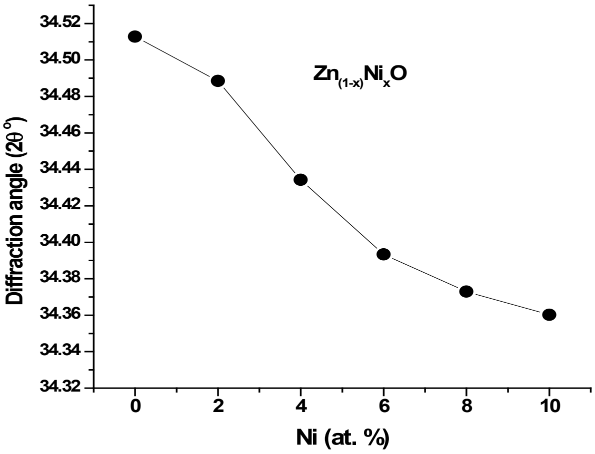

Fig. 4. Diffraction angles as a function of Ni concentration for $Zn_{1-x}Ni_xO$ thin films.

In addition, the full width at half maximum (FWHM) increases with increasing Ni content as shown in Fig. 5. This behavior implies a decrease in crystallite size and thus the crystalline quality of the thin films. The crystallite size (*D)* can be calculated by using Scherrer formula [18, 19]:

$$D = \frac{0.9\lambda}{\beta \cos\theta} \tag{1}$$

where λ is the incident wavelength and β is the structural broadening that equal the difference in integral X-ray peak profile width between the sample and a standard (silicon) and it is given by $\beta = \sqrt{\beta_{obs}^2 - \beta_{std}^2}$.

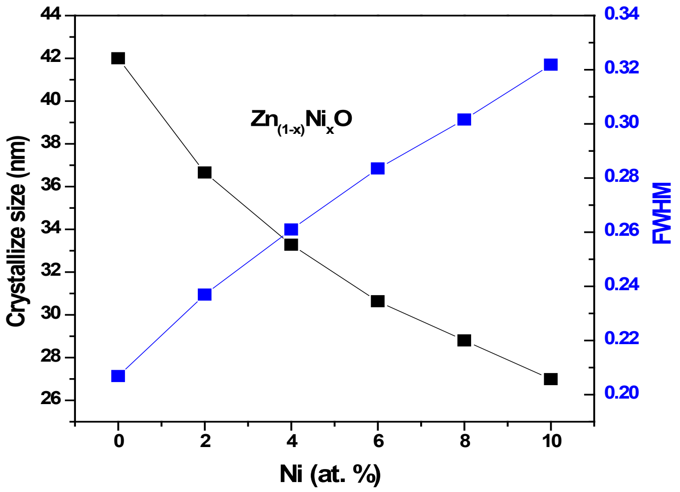

Fig. 5. Crystalline size and FWHM as a function of Ni concentration of $Zn_{1-x}Ni_xO$ thin films.

The *D* values drop as the Ni content rises, as shown in Fig. 5. Ni ions' production of oxygen vacancies that lower lattice parameters and produce significant tensile stress are to blame for the reduction in crystallite size [20]. Additionally, the Ni dopant's inclusion prevents the ZnO particles from adhering together, which reduces the average crystallite size [21].

3.2. Optical Properties

UV-Vis transmission spectra were used to examine the optical characteristics of the Zn1-xGdxO thin films (Fig. 6). All film transmissions show fringes without amplitude shrinkage, especially in the region of medium absorption, which suggests that the deposited films have a homogeneous structure. Additionally, as Ni increases at the expense of Zn in Zn1-xNixO thin films, the absorption edge of the deposited films exhibits a red shift, as shown in the inset of Fig. 6. According to this pattern, the Ni has an impact on the transmission spectra and, consequently, the energy gap of the deposited films.

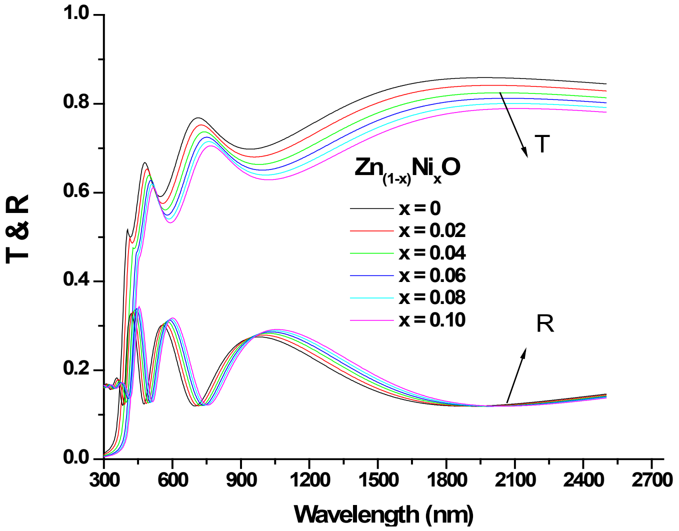

Fig. 6. A typical optical transmission-reflection spectra of $Zn_{1-x}Ni_xO$ thin films.

According to the envelope method of transmission spectrum, the value of refractive index at a certain wavelength can be calculated using the following relationship [22-24]:

$$n = \left[N_1 + (N_1^2 - s^2)^{\frac{1}{2}} \right]^{\frac{1}{2}} \tag{2}$$

where

$$N_1 = 2s \frac{T_M - T_m}{T_M T_m} + \frac{s^2 + 1}{2} \tag{3}$$

where T_M and T_m are the transmittance maximum and the corresponding minimum at a certain wavelength as shown in Fig. 7 for ZnO film.

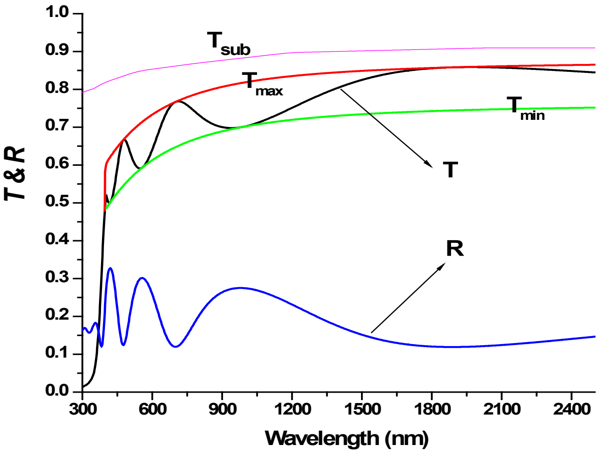

Fig. 7. A typical optical transmission-reflection spectra of ZnO thin film.

The value of the refractive index of the substrate can be obtained from the transmittance spectrum of the substrate (T_s) using the well-known equation [25]:

$$s = \frac{1}{T_s} + \left(\frac{1}{T_s} - 1\right)^{\frac{1}{2}} \tag{4}$$

In terms of the calculated refractive indices n_1 and n_2 at two adjacent maxima (or minima) at λ_1 and λ_2, respectively, the film thickness is given by the relationship:

$$d = \frac{\lambda_1 \lambda_2}{2(\lambda_1 n_{e2} - \lambda_2 n_{e1})} \tag{5}$$

The values of the film thickness of as-deposited and annealed $Zn_{1-x}Ni_xO$ thin films was about 200 ± 2% nm. The refractive index of all these films displays normal dispersion i.e. decrease with increasing wavelength (see Fig. 8) that follows Sellmeier equation [25]:

$$n^2 = 1 + \frac{A_o \lambda^2}{\lambda^2 - \lambda_o^2} \tag{6}$$

Rearrange this equation gives:

$$\frac{1}{n^2-1} = -\frac{A}{\lambda^2} + B \tag{7}$$

where $A = \lambda_0^2 / A_0$ and $B = 1/A_0$

By plotting the relationship between $1/(n^2-1)$ and $1/\lambda^2$ the slope, A and intercept, B can be determined thus λ_o and A_o as well. The Sellmeier coefficient are listed in Table 1, can be used for both interpolation and extrapolation over the whole wavelength range as shown in Fig. 8.

Table 1. The Sellmeier coefficient and energy gap of $Zn_{1-x}Ni_xO$ films.

Ni content (%)	**Sellmeier coefficients**				**E_o (eV)**
	A	**B**	**A_o**	**λ_o (nm)**	
0	4.99744	0.44135	2.134	333.333	3.278
2	4.06818	0.38024	2.47738	324.027	3.175
4	3.30964	0.3298	2.85471	313.731	3.073
6	2.64519	0.29197	3.22719	298.188	2.978
8	2.16698	0.25317	3.71219	289.476	2.925
10	1.73727	0.22407	4.1904	275.418	2.897

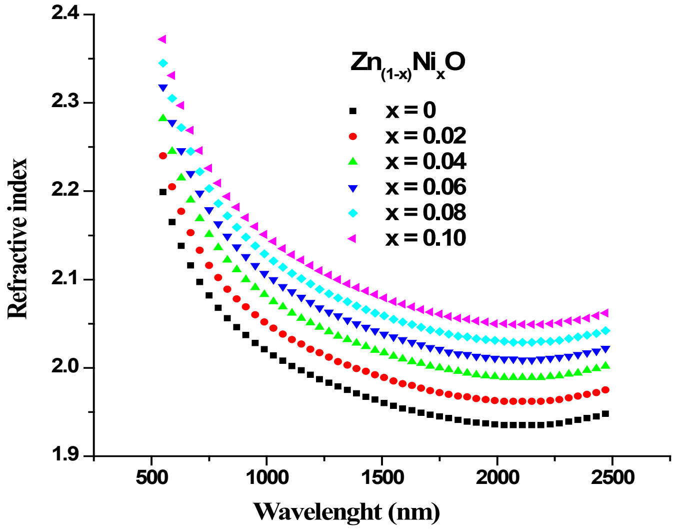

Fig. 8. Dispersion of refractive index of polycrystalline $Zn_{1-x}Ni_xO$ thin films obtained from transmission spectra.

The absorption coefficient (α) of $Zn_{1-x}Ni_xO$ can be calculated in the strong absorption region of transmission spectra using the following relationship:

$$T = \frac{A}{B} e^{-\alpha d} \tag{8}$$

where $A = 16n^2 s$ and $B = (n+1)^3 / (n+s^2)$

In the strong absorption region, the interference fringes disappear and the two curves $T_{\max}$ and $T_{\min}$ converge to a single curve. A and B depend on the refractive index (n) of the thin film and refractive index of the substrate (S). By knowing the value of thickness (*d*), the values of *n* can be extrapolated in the strong absorption region in terms of Sellmeier Eq., thus the absorption coefficient (α) can be calculated using the following expression [26-28]:

$$\alpha = \frac{1}{d}\ln\left(\frac{A}{BT}\right) \tag{9}$$

Fig. 9 shows the variation of α(hν) as a function of hν for $Zn_{1-x}Ni_xO$ films. Absorption of photons causes a transition of the electrons from valence band to conduction band. The absorption ability is measured by its absorption coefficient (α) which is a function of frequency [29-31]. In order to complete the calculation of optical constants, the extinction coefficient, k should be calculated from the relation $\alpha = 4\pi k/\lambda$. Fig. 10 shows the extinction coefficient spectra for $Zn_{1-x}Ni_xO$ films, the inset of the Fig. 10 shows the amplification of extinction coefficient in the strong absorption region and its increasing with increasing of Ni content and also displays a red shift of the spectra (band gap).

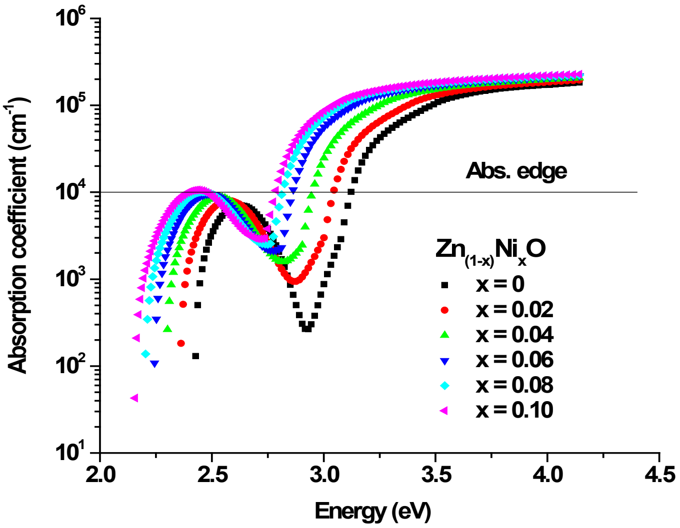

Fig. 9. The absorption coefficient versus photon energy for the polycrystalline $Zn_{1-x}Ni_xO$ thin films.

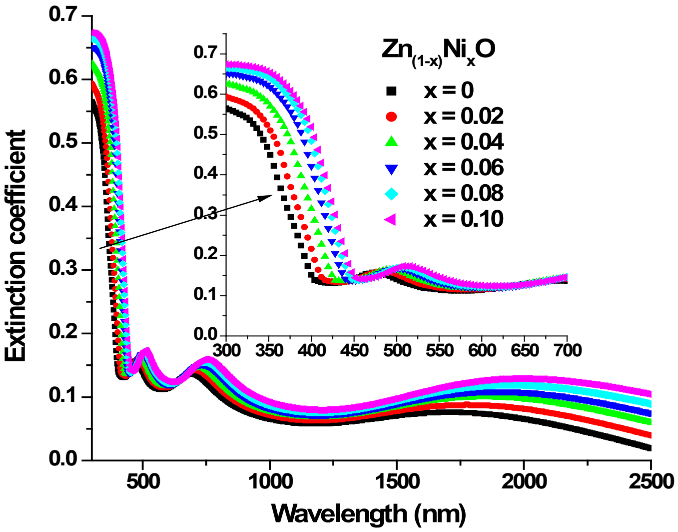

Fig. 10. The extinction coefficient spectra for the polycrystalline $Zn_{1-x}Ni_xO$ thin films.

For allowed direct band-to-band transitions, the α(hν) is described as:

$$\alpha(h\upsilon)=\frac{\beta(h\upsilon-E_g^{opt})^m}{h\upsilon} \tag{10}$$

where β is a characteristic parameter (independent of photon energy) for respective transitions and m is a number that characterizes the transition process. m = 2 for most amorphous semiconductors (indirect transition) and m =1/2 for most crystalline semiconductor (direct transition) [32-35]. According to polycrystalline nature of the XRD films, as shown in Fig. 3, thus the allowed direct optical band gaps of $Zn_{1-x}Ni_xO$ are evaluated from $(\alpha h\nu)^2$ against hν plot and extrapolated to intersect the energy axis at $(\alpha h\nu)^2 = 0$ gives the direct E_g^{opt} (see Fig. 11).

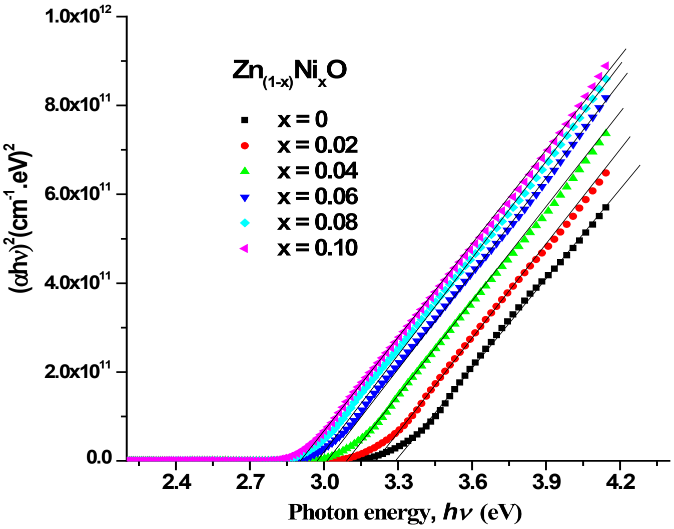

Fig. 11. The dependence of $(\alpha h\nu)^2$ *on photon energy for the different compositions of* $Zn_{1-x}Ni_xO$ *thin films.*

The variation of direct E_g^{opt} as a function of Ni content is shown in Fig. 12. The values of direct E_g^{opt} are found to decrease with increasing Ni content (see Table 1). This indicates that the doping ions introduce new electronic levels (subbands) inside the ZnO band-gap. These new electronic levels were merged with the conduction band forming continuous band leading to the reduction of the band gap. In addition, the red shift in band gap may be related to the presence of defects such as oxygen vacancies and interstitial oxygen, which certainly are inherent to the synthesis process [36, 37].

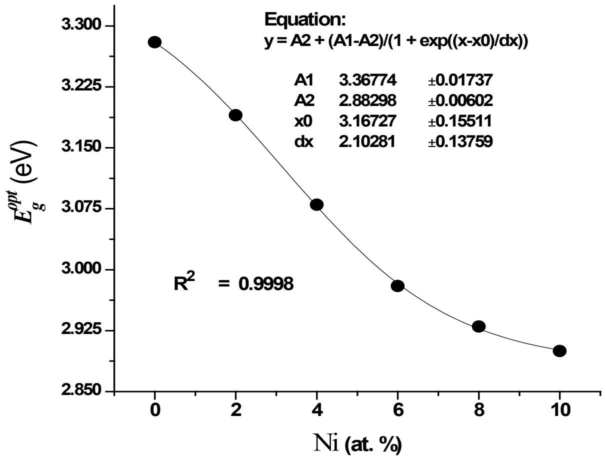

Fig. 12. Variation in optical energy gap as a function of Ni content.

The decrease in E_g^{opt} for direct transition may be attributed to the decrease in the crystallite size because the crystal defects can be formed which produce localized states that change the effective Fermi level due to an increase in carrier concentration [38, 39].

3.3. Magnetic properties

By applying parallel magnetic fields to the film planes at RT, the magnetic characteristics of thin films of $Zn_{(1-x)}Ni_xO$ were examined. Fig. 13 shows the hysteresis M-H plots for the magnetization measurements M(H) against the magnetic field for the $Zn_{(1-x)}Ni_xO$ thin films. All of the results were collected after the diamagnetic contribution from the glass substrates was removed. The magnetization plot of pure ZnO exhibits a diamagnetic-like behaviour with a negative magnetic susceptibility [24], as would be predicted given its inherent diamagnetic nature. Figure 13 shows the M-H curves for doped $Zn_{(1-x)}Ni_xO$ films at RT. The magnetism in doped ZnO: Ni films may be the result of interactions, as this figure demonstrates a hysteretic trend and reveals a ferromagnetic characteristic with a tiny coercive field and low remanence of soft ferromagnetism.

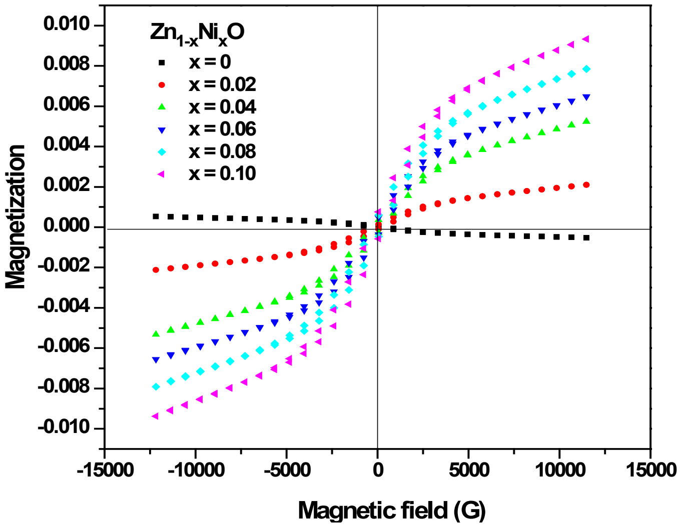

Fig. 13. Magnetization hysteresis loops for the different compositions of $Zn_{1-x}Ni_xO$ thin films.

The source of ferromagnetism in Ni doped ZnO, a diluted magnetic semiconductor (DMS) with a modest fraction of up to 10%, is still a contentious issue that is not entirely clear. The increase in saturation magnetization can be attributed to oxygen vacancies, which generates long range ferromagnetism as the doping of Ni ions, in turn; increase the oxygen [40]. However, two precise mechanisms resulting from a number of theories are frequently expected to explain the ferromagnetism of DMSs: the carrier-induced Ruderman-Kittel-Kasuya-Yosida substitute interaction (RKKY interaction) or bound magnetic polarons (BMPs) producing long-range magnetic order [41, 42]. The purpose of the current work is to investigate the mechanism by which the carrier causes ferromagnetism (dual exchange mechanism) in Ni-doped ZnO films. It is possible that the substitution of Ni ions for Zn ions is what caused the ferromagnetic behaviour observed in the ZnO lattice. A similar effect was observed in Co-doped ZnO [43] and Er-doped ZnO [44] systems.

4. Conclusions

Co-precipitation method was used to prepare different compositions of the bulk sample of $Zn_{1-x}Ni_xO$ (x = 0, 0.02, 0.04, 0.06, 0.08 and 0.1) and then deposited as thin films onto highly-clean glass substrates by electron beam technique. The structural, optical and magnetic properties of ZnO thin films doped by Ni were investigated in details. The films show formation of hexagonal wurtzite single phase of ZnO and having intense (002) peak with a peak shift towards lower angle.

The crystallite size of the films was found to be decreased from 42 nm to 25 nm with increasing Ni content from 0 to 0.1. The optical energy gap decreases from 3.28 to 2.90 eV with increasing Ni content. In addition, magnetic tests at RT revealed ferromagnetism in all Ni-doped ZnO films. It is possible to attribute the ferromagnetic behaviour seen in the ZnO lattice to the substitution of Zn ions by Ni ions. The increase in saturation magnetization can be attributed to oxygen vacancies, which generates long range ferromagnetism as the doping of Ni ions, in turn; increase the oxygen.

Acknowledgments

The Deanship of Scientific Research (DSR) at King Abdulaziz University, Jeddah, Saudi Arabia has funded this project, under grant no. (RG-104-130-42).

References

[1] M. Bouloudenine, N. Viart, S. Colis, J. D. Kortus, Appl. Phys. Lett. 87 (2005) 052501; https://doi.org/10.1063/1.2001739

[2] A. S. Risbud, N. A. Spaldin, Z. Q. Chen, S. S. Stemmer, Phys. Rev. B 68 (2003) 205202; https://doi.org/10.1103/PhysRevB.68.205202

[3] S. Thota, T. Dutta, J. Kumar, J. Phy.s: Condens. Matter. 18 (2006) 2473; https://doi.org/10.1088/0953-8984/18/8/012

[4] S. J. Pearton, C. R. Abernathy, M. E. Overberg, G. T. Thaler, D. P. Norton, J. Appl. Phys. 93 (2003) 1; https://doi.org/10.1063/1.1517164

[5] X. Wang, J. Xu, B. Zhang, H. Yu, J. Wang, X. Zhang, J. Yu, Q. Li, Adv. Mater. 18 (2006) 2476; https://doi.org/10.1002/adma.200600396

[6] G. Vijayaprasath, R. Murugan, T. Mahalingam, Y. Hayakawa, G. Ravi, Ceram. Int. 41 (2015) 10607-10615; https://doi.org/10.1016/j.ceramint.2015.04.160

[7] S. Chambers, Nat. Mater. 9 (2010) 956; https://doi.org/10.1038/nmat2905

[8] G. Vijayaprasath, R. Murugan, T. Mahalingam, Y. Hayakawa, G. Ravi, J. Alloys Comp., 649 (2015) 275; https://doi.org/10.1016/j.jallcom.2015.07.089

[9] I. Khan, S. Khan, R. Nongjai, H. Ahmed, W. Khan, Opt.Mater. 35 (2013) 1189-1193; https://doi.org/10.1016/j.optmat.2013.01.019

[10] F. Ahmed, S. Kumar, N. Arshi, M.S. Anwar, S.N. Heo, B.H. Koo, ActaMater. 60 (2012) 5190-5196; https://doi.org/10.1016/j.actamat.2012.06.033

[11] W. Huang, X. Tanga, I. Felnerb, Y. Koltypin, A. Gedanken, Mater. Res. Bul. 37(2002) 1721-1735; https://doi.org/10.1016/S0025-5408(02)00821-8

[12] C.R. Estrellan, C. Salim, H. Hinode, React. Kinet. Catal. Lett. 98 (2009) 187-192; https://doi.org/10.1007/s11144-009-0061-x

[13] P. Sahay, S. Tewari, R. Nath, S. Jha, M. Shamsuddin, J. Mater. Sci. 43 (13) (2008) 4534-4540; https://doi.org/10.1007/s10853-008-2642-x

[14] J. Jose, M. Abdul Khadar, Mater. Sci. Eng. A 304 (2001) 810-813; https://doi.org/10.1016/S0921-5093(00)01579-3

[15] K. Raja, P.S. Ramesh, D. Geetha, Synthesis, Spectrochim. Acta Part A: Mol. Biomol. Spectrosc. 120 (2014) 19-24; https://doi.org/10.1016/j.saa.2013.09.103

[16]Emam-Ismai M l, El-Hagary M, Shaaban E.R., Althoyaib S, Journal of alloys and compounds 2012, 529, 113-121; https://doi.org/10.1016/j.jallcom.2012.03.027

[17] ER Shaaban, YAM Ismail, HS Hassan, Journal of non-crystalline solids 376, 61 (2013); https://doi.org/10.1016/j.jnoncrysol.2013.05.024

[18] A. L. Patterson, Phys. Rev. 56 (1939) 978; https://doi.org/10.1103/PhysRev.56.978

[19] O. A. Fouad, S. A. Makhlouf, G. A. M. Ali, A. Y. El-Sayed, Mater. Chem. Phys. 128 (2011) 70-76; https://doi.org/10.1016/j.matchemphys.2011.02.072

[20] A. A. Dakhel, M. El-Hilo, J. Appl. Phys. 107 (2010) 123905; https://doi.org/10.1063/1.3448026

[21] A. Khataee, R. D. C. Soltani, A. Karimi, S. W. Joo, Ultrason. Sonochem. 23 (2015) 219; https://doi.org/10.1016/j.ultsonch.2014.08.023

[22] E. R. Shaaban, A. Almohammedi, E. S. Yousef, G. A. M. Ali, K. F. Chong, A. Adel, A. Ashour, Optik 164 (2018) 527; https://doi.org/10.1016/j.ijleo.2018.03.001

[23] R. Swanepoel, J. Phys. E: Sci. Instrum. 16 (1983) 121; https://doi.org/10.1088/0022-3735/16/12/023

[24] E. R. Shaaban, I. S. Yahia, E. G. El-Metwally, Acta Phys. Pol. A 121 (2012) 628; https://doi.org/10.12693/APhysPolA.121.628

[25] T. Bellunato, M. Calvi, C. Matteuzzi, M. Musy, D. L. Perego, B. Storaci, Europ. Phys. J. 52 (2007) 759; https://doi.org/10.1140/epjc/s10052-007-0431-3

[26] F. A. Jenkins, H. E. White, J. Phys. E: Sci. Instrum. 16 (1983) 1214; https://doi.org/10.1088/0022-3735/16/12/023

[28] E. Marquez, J. B. Ramirez-Malo, P. Villares, R. Jimenez-Garay, R. Swanepoel, Thin Solid Films 234 (1995) 83; https://doi.org/10.1016/0040-6090(94)06267-O

[29] Y. E. Lee, Y. J. Kim, H. J. Kim, J. Mater. Res. 13 (1998) 1260; https://doi.org/10.1557/JMR.1998.0180

[30] H. Tabet-Derraz, N. Benramdane, D. Nacer, A. Bouzidi, M. Medles, Sol. Energy Mater. Solar Cells. 73 (2002) 248; https://doi.org/10.1016/S0927-0248(01)00134-9

[31] L. F. Dong, Z. Cui, Z. K. Zhang, Nanostru. Mater. 8 (1997) 815; https://doi.org/10.1016/S0965-9773(98)00005-1

[32] E. A. Davis, N. F. Mott, Philos. Mag. 22 (1970) 903; https://doi.org/10.1080/14786437008221061

[33] E. A. Davis, N.F. Mott, Philos. Mag. 22 (1970) 903; https://doi.org/10.1080/14786437008221061

[34] E. R. Shaaban, Philos. Mag. 88 (2008) 781; https://doi.org/10.1080/14786430801968595

[35] E. R. Shaaban, M. Abdel-Rahman, E. Yousef, M. T. Dessouky, Thin Solid Films 515 (2007) 3810; https://doi.org/10.1016/j.tsf.2006.10.012

[36] E. R. Shaaban, Appl. Phys. A 115 (2014) 919; https://doi.org/10.1007/s00339-013-7889-7

[37] E. R. Shaaban, J. Alloys Compds. 563 (2013) 274; https://doi.org/10.1016/j.jallcom.2013.02.132

[38] G. L. Kabongo, G. H. Mhlongo, T. Malwela, B. M.Mothudi, K. T. Hillie, M. S. Dhlamini, J. Alloys Compds. 591 (2014) 156; https://doi.org/10.1016/j.jallcom.2013.12.075

[39] K. Kaur, G. S. Lotey, N. K. Verma, J. Mater. Sci.: Mater. Electron. 25 (2014) 2605; https://doi.org/10.1007/s10854-014-1918-y

[40] S. Kumar, P.D. Sahare, Mater. Res. Bull. 51 (2014) 217; https://doi.org/10.1016/j.materresbull.2013.12.031

[41] J. Coey, M. Venkatesan, C. Fitzgerald.. Nat Mater. 4(2): (2005)173; https://doi.org/10.1038/nmat1310

[42] S. Ramachandran, J. Narayan, J. Prater. Appl Phys Lett. 88(24): (2006) 242503; https://doi.org/10.1063/1.2213930

[43] M. Venkatesan, C. B. Fitzgerald, J. G. Lunney, J. M. D. Coey, Phys. Rev. Lett. 93 (2004) 177206; https://doi.org/10.1103/PhysRevLett.93.177206

[44] J. Qi, Y. Yang, L. Zhang, J. Chi, D. Gao, D. Xue, Scr. Mater. 60 (2009) 289; https://doi.org/10.1016/j.scriptamat.2008.10.015